ISSN 1069-3513, Izvestiya, Physics of the Solid Earth, 2006, Vol. 42, No. 4, pp. 297–306. © Pleiades Publishing, Inc., 2006.
Original Russian Text © A.A. Lyubushin, 2006, published in Fizika Zemli, 2006, No. 4, pp. 30–39.

Wavelet Packet Polarization Method for an Automatic Detection of *P* and *S* Wave Arrivals

A. A. Lyubushin

Schmidt Institute of Physics of the Earth, Russian Academy of Sciences, Bol'shaya Gruzinskaya ul. 10, Moscow, 123995 Russia

Received April 26, 2005

Abstract—A new method is proposed for detecting *P* and *S* wave arrivals in the problem of passive seismic monitoring. This method is based on the wavelet packet decomposition of three-component seismic traces, their automatic quality control, and the calculation of the principal components of the traces in overlapping packet frequency bands and in scale-dependent moving time windows. The wave arrivals times are estimated by means of a robust iterative procedure of adjusting hyperbolic traveltime curves to the initial estimates of arrival times determined from the maximum values of the multilevel measure of the nonstationarity of each trace. The method has been developed for applications in the cases of a large number of bad single-component traces and a high noise level. To illustrate its application, the method is applied to the data set of the Cotton Valley experiment on the seismic monitoring of hydraulic fractures in a fractured gas reservoir.

PACS numbers: 91.30.Cd

DOI: 10.1134/S1069351306040045

INTRODUCTION

The determination of *P* and *S* wave arrivals and their traveltime curves is one of the most routine problems in seismic data analysis [*Seismic Signal …*, 1982; Hatton et al., 1986; Pisarenko et al., 1987; Gashin and Kushnir, 1998; Kushnir and Khaikin, 2000]. Large amounts of seismic data, particularly in problems of seismic monitoring of weak events and seismic exploration, involving a high noise level and large numbers of bad traces, makes it very important to automate the detection of wave arrivals. In this paper, we propose a new method for solving this problem based on the use of compact orthogonal basis functions (wavelets) [Chui, 1992; Daubechies, 1992; Mallat, 1998; Press et al., 1996] for the decomposition of initial signals and adaptive analysis of the principal components to suppress noise. The well known advantages of wavelet analysis over the classic Fourier expansion are due to the compactness of basis functions. The application of wavelet analysis to seismic data treatment makes it possible to develop new methods for the identification and classification of signals [Lyubushin et al., 2004]. One of the shortcomings of using orthogonal wavelets is their low resolution in frequency, which is the flip side of their good resolution in time. An increase in the frequency resolution of wavelet analysis in the paper is achieved by using so-called wavelet packets. Note that the method proposed here can be realized with the use of ordinary bandpass Fourier filtering, but the result will then be much less accurate and stable.

METHOD

Below, the method is successively described with parallel examples of real data treatment. This form of presentation appears to be more appropriate for understanding all the elements of the method as compared with the conventional form (a formal description of the method followed by the results of its application). The data we used are seismograms from the database of the Cotton Valley, East Texas field experiment on the identification of events (hydraulic fractures, i.e., crack openings caused by hydraulic pressure) initiated by high-pressure water injection into a gas reservoir [Maxwell et al., 1998, 2000; Zinno et al., 1998]. The events were recorded upon the attenuation of transient processes following the water injection by a system of three-component (3C) geophones mounted in a borehole at 50-m intervals. The sampling frequency was 1000 Hz, the total number of geophones was 45, and the number of samples in each scalar (1C) trace was 400. Initial data are presented in Fig. 1 separately for the *X*, *Y*, and *Z* components. A number increasing from 1 to 45 in proportion to the geophone depth is ascribed to each 3C record. The data were provided for testing the method by Dr. David Leslie of the Schlumberger Cambridge Research Center.

This example of data is typical of the experiment. As can be easily seen, the data contain a large number of bad 1C traces. On the other hand, there are many 3C records in which not all of the components are bad. Thus, it is necessary to develop a method for automatic rejection of bad 1C traces. Qualitatively, 3C records can be classified as "bad" (all three scalar traces are bad),

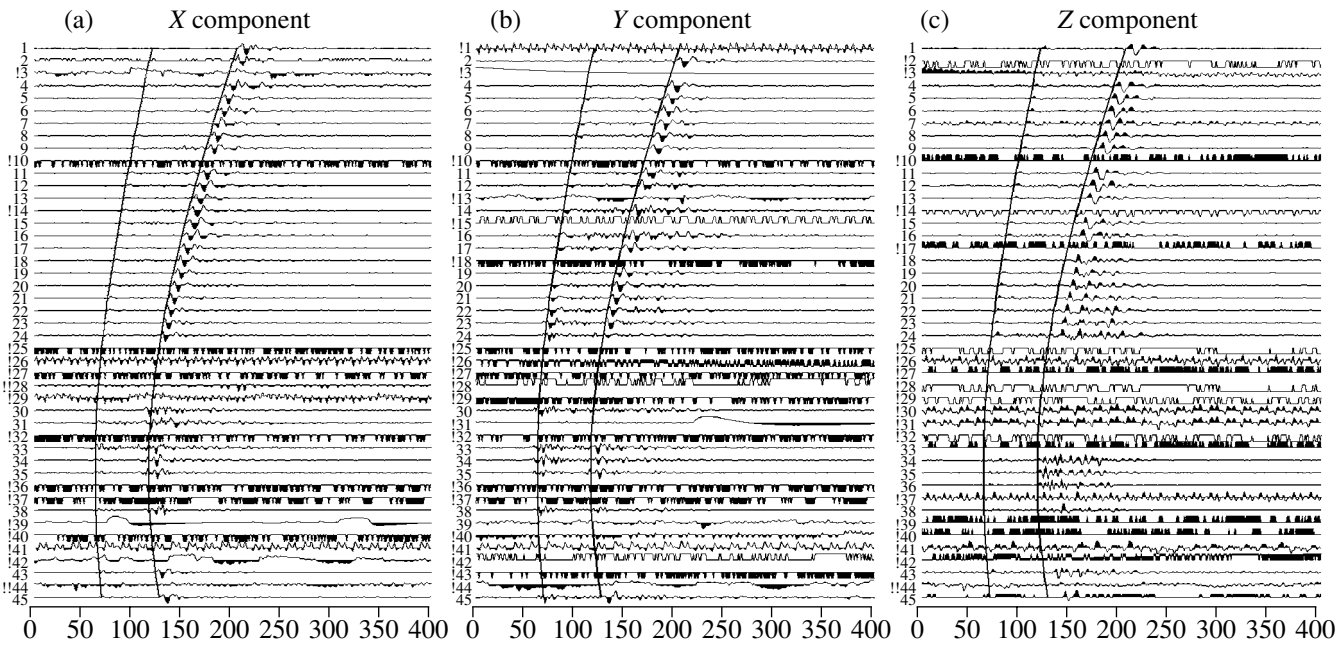

Fig. 1. Initial data: (a) *X* component; (b) *Y* component; (c) *Z* component. The horizontal axis shows the numbers of time samples (a sampling frequency of 1000 Hz); the vertical axis shows the numbers of traces corresponding to three-component geophones mounted in a vertical borehole at 50-m intervals. A single exclamation mark indicates scalar traces identified as bad at the first stage of the automatic quality control; a double exclamation mark indicates scalar traces identified as bad at the second stage of automatic quality control. Each plot shows the lines of hyperbolic traveltime curves of arrival times, first for *P* waves and then for *S* waves.

"partially good" (if one or two scalar traces are suitable for subsequent analysis), and "good." Below, 1C traces will be designated as X-21, Z-02, Y-14, and so on, with obvious mnemonics: the letter indicates the component, and the number specifies the 3C trace in Fig. 1. The method must not reject all information contained in a 3C record if one or even two scalar components are bad: any adequate 1C trace must be used. If a 3C trace is good or contains two good 1C traces, it is possible to use the method of principal components for additional noise suppression. In the case of 3C seismic records, the method of principal components is none other than polarization analysis [Kanasewich, 1981].

The method consists of the following sequence of operations:

(1) wavelet packet decomposition of all 1C traces;

(2) estimation of variations in the multilevel measure of nonstationarity for all 1C traces;

(3) quality control of 1C traces with the use of the multilevel measure from step (2), the normalized entropy of the distribution of the squared wavelet coefficients, and the criterion of the high-to-low frequency energy ratio for marking automatically bad 1C traces;

(4) calculation of adaptive principal components for all good or partially good 3C traces in overlapping wavelet packet frequency bands and in scale-dependent moving time windows;

(5) estimation of variations in the multilevel measure of nonstationarity for all scale-dependent principal components;

(6) determination of the initial estimates of *S* wave arrival times using maximum values of the nonstationarity measures calculated at step (5);

(7) correction of the initial estimates of *S* wave arrival times and identification of the hyperbolic *S* wave traveltime curve using an iterative robust procedure for adjusting parameters of the curve;

(8) determination of the initial estimates of *P* wave arrival times using maximum values of the nonstationarity measures calculated at step (5) for time moments strictly before the *S* arrival times determined at step (7);

(9) correction of the initial estimates of *P* wave arrival times and identification of the hyperbolic *P* wave traveltime curve using an iterative robust procedure for adjusting parameters of the curve.

Each of the above steps is described in detail below. In addition to the initial data, Fig. 1 also shows the final estimates of the *P* and *S* wave traveltime curves. All other figures (Figs. 2–6) illustrate the particulars of the above sequence of operations.

1. Wavelet packet decomposition. Orthogonal wavelet decomposition of a signal $x(t)$ with the discrete

time index $t = 1, \ldots, N$ gives its representation as the sum

$$x(t) = \text{const} + \sum_{\beta=1}^{m} x^{(\beta)}(t), \quad (1)$$

where $x^{(\beta)}(t)$ is the signal component belonging to the detail level with the number β [Chui, 1992; Daubechies, 1992; Mallat, 1998; Press et al., 1996]. The total number m of detail levels depends on the length N of the signal in a number of samples. If $N = 2^n$, then $m = n$ and the number of wavelet coefficients is equal to $N/2$ at the 1st level, $N/4$ at the 2nd level, and so on, up to the mth detail level, which has a single coefficient of decomposition. If N is not equal to 2^m, we add zeros to the signal $z(t)$ until its length becomes equal to 2^m, where m is the minimum integer for which $N \le 2^m$. The component $x^{(\beta)}(t)$ for a sufficiently large value of N is localized in the frequency band

$$[\Omega_{\min}^{(\beta)}, \Omega_{\max}^{(\beta)}] = [1/(2^{(\beta+1)}\Delta t), 1/(2^{\beta}\Delta t)], \quad (2)$$

where Δt is the length of the time sampling interval (10^{-3} s in our case). The relationship between the wavelet decomposition coefficients and the initial data set is described in detail in [Chui, 1992; Daubechies, 1992; Mallat, 1998; Press et al., 1996; Lyubushin, 2000, 2002].

A distinctive feature of formula (1) for wavelet decomposition (note that the same or similar formula can also be written when using multiband Fourier filtering) is precisely the use of the complete orthogonal basis of compactly supported functions. In this case, the influence of short-lived pulsations (in both noise and useful signals) is inevitably limited in time, whereas the use of a basis of sines and cosines, due to the unboundedness of their support, results in side effects of filtering (particularly, for signals with a small number of samples) that lead to "globalization" of the influence of local pulsations on the entire time interval being processed. Ultimately, these side effects lead to the postfiltering spread of seismic wave fronts and reduce the accuracy of the arrival time determination.

Although ordinary wavelet decomposition has the useful property of high accuracy in localizing nonstationary signals in the time domain, the flip side of this property is, in accordance with the Heisenberg principle, a low frequency resolution. The wavelet packet decomposition can partially eliminate this shortcoming at the expense of a certain decrease in the time resolution. The realization of packet decomposition is based on a hierarchical scheme of successive transforms of initial coefficients (wavelet transforms of sequences of wavelet coefficients). The orthogonal wavelet packet splitting of the signal, similarly to formula (1), can be written as the sum

$$x(t) = \text{const} + \sum_{\beta=1}^{m_q}\sum_{\gamma=1}^{q} x^{(\beta,\gamma)}(t) + \sum_{\beta=m_q+1}^{m} x^{(\beta)}(t). \quad (3)$$

The quantity q can be equal to 2, 4, 8, …; i.e., it has the form $q = 2^r$, $r = 1, 2, \ldots$, and defines the number of sublevels into which the ordinary detail level is split. For a given value of q, the maximum number $m_q < m$ of the detail level β that can be split is determined from the condition that it must contain the minimum q of wavelet coefficients. The components $x^{(\beta,\gamma)}(t)$ are frequency-ordered and split frequency band (2) corresponding to the detail level β into q equal parts. Thus, the signal $x^{(\beta,\gamma)}(t)$ is localized in the frequency band

$$\begin{gathered}[\Omega_{\min}^{(\beta,\gamma)}, \Omega_{\max}^{(\beta,\gamma)}],\ \Omega_{\min}^{(\beta,\gamma)} = \Omega_{\min}^{(\beta)} + (\gamma-1)\Delta\Omega^{(\beta)},\\ \gamma = 1, \ldots, q;\\ \Omega_{\max}^{(\beta,\gamma)} = \Omega_{\min}^{(\beta,\gamma)} + \Delta\Omega^{(\beta)},\\ \Delta\Omega^{(\beta)} = (\Omega_{\max}^{(\beta)} - \Omega_{\min}^{(\beta)})/q.\end{gathered} \quad (4)$$

Below, we use only the value $q = 8$. In this case, the component $x^{(\beta,\gamma)}(t)$ will be referred to as the γth octave of the detail level with the number β. For wavelet packet decomposition, we use the eighth-order Daubechies basis function, which nullifies the first four moments, which have eight nonzero coefficients in the discrete time filter (used to calculate both the coefficients of decomposition and the components in formulas (1) and (3)). This choice is the result of a large number of experiments with wavelets of various orders with automatic wavelet selection using criteria of the entropy minimum type [Mallat, 1998]. A value of 8 for the wavelet order proved to be best for the seismic data analysis: its basis function is both sufficiently compact (with increasing order, its support expands) and sufficiently smooth (a decrease in the order gives rise to discontinuities of derivatives in the compactly supported basis function).

The wavelet packet decomposition isolates the components of the signal in overlapping frequency bands consisting of a given number p of adjacent octaves that can belong to different detail levels. These wavelet packet frequency bands are displaced relative to each other by one octave and give detailed frequency–time decomposition of the signal. Let p be the number of adjacent octaves. Then, we can ascribe the integral index $\alpha = 1, \ldots, \alpha_{\max}$ to consecutively overlapping wavelet packet frequency bands of a length of p octaves with gradually increasing boundaries of the maximum ($T_{\max}^{(\alpha)}$) and minimum ($T_{\min}^{(\alpha)}$) periods. The values (p, $\alpha_{\max}$) are the parameters of the method and define the frequency resolution (the parameter p) and the frequency range (the parameter $\alpha_{\max}$) of the wavelet packet analysis. To process the data set used as an example, we chose the values $p = 6$ and $\alpha_{\max} = 17$. The

Values of the minimum and maximum periods of the first 17 overlapping wavelet packet frequency bands with a length of six octaves

Band number α	Period $T_{\min}^{(\alpha)}$	Period $T_{\max}^{(\alpha)}$	Band number α	Period $T_{\min}^{(\alpha)}$	Period $T_{\max}^{(\alpha)}$
1	2.000	3.200	10	4.267	7.111
2	2.133	3.556	11	4.571	8.000
3	2.286	4.000	12	4.923	8.533
4	2.462	4.267	13	5.333	9.143
5	2.667	4.571	14	5.818	9.846
6	2.909	4.923	15	6.400	10.667
7	3.200	5.333	16	7.111	11.636
8	3.556	5.818	17	8.000	12.800
9	4.000	6.400			

table presents the correspondences between the minimum and maximum periods of the frequency bands for the selected values of the parameters p and $\alpha_{\max}$ measured in units of the length of the sampling interval Δt.

Let

$$z_{j,k}(t),\ j = 1, \ldots, N_{\text{tr}};\ k = 1, 2, 3;\ t = 1, \ldots, L \quad (5)$$

denote the set of all 1C seismic traces. Here, N_{tr} is the total number of 3C records (45 in our case); L is the number of samples in each 1C trace (400 in our case); and the index $k = 1$, 2, and 3 corresponds to the *X, Y,* and *Z* components. Thus, the first operation of the method is to calculate the matrix

$$z_{j,k}^{(\alpha)}(t),\quad \alpha = 1, \ldots, \alpha_{\max}, \quad (6)$$

corresponding to the system of overlapping frequency bands. Figure 2a plots the initial 1C trace X-21 ($j = 21$, $k = 1$), and Fig. 2b shows its decomposition (6).

2. Multilevel measure of nonstationary behavior. Let $z_{j,k}^{(\alpha)}(t)$ denote any component of the αth frequency band of the scalar seismic trace $z_{j,k}(t)$. We take a moving time window having the radius $M^{(\alpha)} = \text{int}(T_{\max}^{(\alpha)})$ of samples with the central point τ and calculate the variance of the component of the αth band in the left and right halves of the moving window:

$$(\sigma_{j,k}^{(\alpha)}(\tau|L))^2 = \sum_{t=\tau-M^{(\alpha)}}^{\tau-1} (z_{j,k}^{(\alpha)}(t))^2/M^{(\alpha)},$$
$$(\sigma_{j,k}^{(\alpha)}(\tau|R))^2 = \sum_{t=\tau+1}^{\tau+M^{(\alpha)}} (z_{j,k}^{(\alpha)}(t))^2/M^{(\alpha)}. \quad (7)$$

Calculating the difference between the variances, we sum these differences over all bands:

$$\mu_{j,k}^{(\alpha)}(\tau) = [(\sigma_{j,k}^{(\alpha)}(\tau|L))^2 - (\sigma_{j,k}^{(\alpha)}(\tau|R))^2]^2,$$
$$\mu_{j,k}(\tau) = \sum_{\alpha=1}^{\alpha_{\max}} \mu_{j,k}^{(\alpha)}(\tau). \quad (8)$$

If statistic (8) has a local minimum for a certain value of τ, this means that the behavior patterns of the signal $z_{j,k}(t)$ to the left and to the right of the point τ sig-

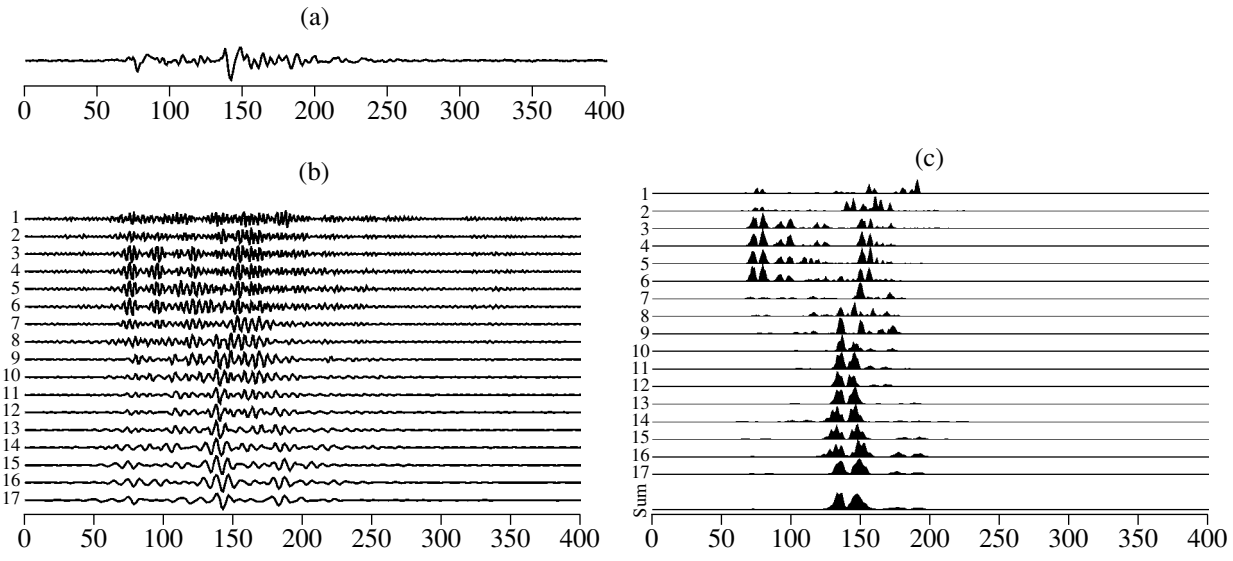

Fig. 2. (a) Good trace X-21. (b) Its representation in 17 overlapping wavelet-packet frequency bands six octaves wide. (c) Behavior of nonstationarity measures in each of the frequency bands; the lowermost plot (marked as "Sum") is the sum of the nonstationarity measures over all frequency bands and demonstrates the presence of arrival signals dominated by the *S* wave.

nificantly diverge. The summation in formula (8) ensures the suppression of strong noise components uncorrelated with each other in different frequency bands, so that the summation results in their mutual suppression. However, some components of the arrival signal are correlated in the majority of bands, and the summation only strengthens pulsations in statistic (8) related to arrival times. Figure 2c presents plots of $\mu_{j,k}^{(\alpha)}(\tau)$ and $\mu_{j,k}(\tau)$ for the trace X-21. Note that the variations in these measures for good seismic traces usually take the form of two closely spaced peaks; this is quite natural because the first peak marks the onset of the wave arrival and the second peak marks its completion.

3. Quality control of 1C traces. The procedure of automatic quality control of 1C traces uses three criteria. The first criterion is based on the calculation of the values

$$\kappa_{j,k} = \frac{\text{median}_\tau\{\mu_{j,k}(\tau)\}}{\max_\tau\{\mu_{j,k}(\tau)\}}. \quad (9)$$

For good scalar traces, the median of statistic (8) is determined by small background values, whereas its maximum values correspond to wave arrivals and considerably exceed the background. Therefore, the value of (9) must be sufficiently small for good traces but large for bad traces with chaotic or periodic behavior of the signal. Thus, if

$$\kappa_{j,k} \geq \kappa_{\max}, \quad (10)$$

then, the 1C trace is classified as bad. The threshold $\kappa_{\max}$ is a parameter of the method, and we used the value $\kappa_{\max} = 0.04$ in our example. Figure 3 shows the scalar trace X-41, which is regarded as bad according to criterion (10).

The second criterion of quality is based on calculating the normalized entropy of the distribution of the squared ordinary wavelet coefficients of the signal at the first and the second detail levels. The normalized entropy of a finite discrete distribution of probabilities $p_i \geq 0$, $i = 1, \ldots, n$, $\sum_{i=1}^{n} p_i = 1$, is defined by the formula

$$\text{En} = \left(-\sum_{i=1}^{n} p_i \ln(p_i)\right)/\ln(n). \quad (11)$$

Thus, the values of En lie between 0 and 1. If p_i is set equal to squared wavelet coefficients for the first and the second detail levels divided by the sum of all these values and n is taken to be equal to the total number of wavelet coefficients at the first two detail levels (at $N = 2^n$, this number is $n = 3N/4$), the value of (11) is then the second criterion $\text{En}_{j,k}$ for the entropy of the 1C trace $z_{j,k}(t)$. If the trace shows chaotic high-frequency behavior ("trembling"), the value of $\text{En}_{j,k}$ is high. In other words, if

$$\text{En}_{j,k} \geq \text{En}_{\max}, \quad (12)$$

the 1C trace is classified as bad. For the analysis of the experimental data performed below, we use the threshold $\text{En}_{\max} = 0.25$.

The third type of bad 1C traces can be called "inflated" (e.g., X-03, X-39, and X-42); they are characterized by an overly high intensity of low frequencies and are identified by using the criterion of the low-to-high frequency energy ratio. Let $E_{j,k}^{(L)}$ denote the sum of the squared wavelet coefficients at all detail levels with numbers $\beta > 3$, and let $E_{j,k}^{(H)}$ be the sum of squared coef-

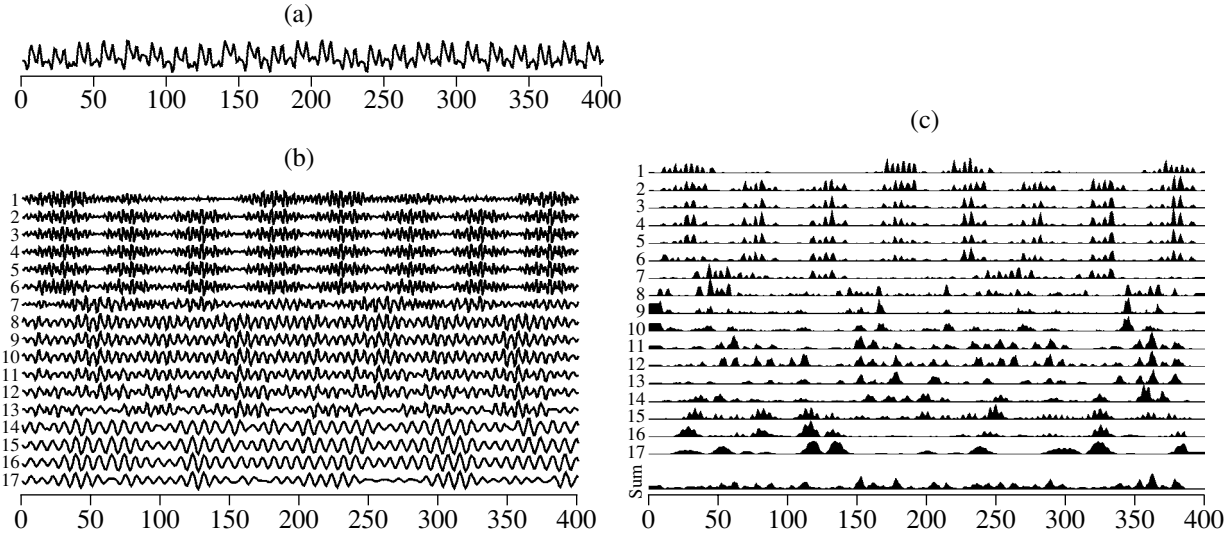

Fig. 3. (a) Bad trace X-41. (b) Its representation in 17 overlapping wavelet-packet frequency bands six octaves wide. (c) Behavior of nonstationarity measures in each frequency band; the lowermost plot (marked as "Sum") is the sum of the nonstationarity measures over all frequency bands and demonstrates chaotic behavior.

ficients at the first to third detail levels of the ordinary (not packet) wavelet decomposition of the 1C trace $z_{j,k}(t)$. We mean the ratio

$$\lambda_{j,k} = E^{(L)}_{j,k}/E^{(H)}_{j,k}, \quad (13)$$

which must be high for bad traces of the third type. Thus, if

$$\lambda_{j,k} \geq \lambda_{\max}, \quad (14)$$

the 1C trace is considered bad. Below, we use the threshold $\lambda_{\max} = 2.75$. If at least one of inequalities (10), (12), or (14) is valid, the 1C trace is classified as bad and is excluded from the subsequent analysis. The scalar traces in Fig. 1 that are marked by a single exclamation mark "!" were identified as bad at the stage of the preliminary quality control.

4. Scale-dependent principal components. Three-component traces all scalar components of which are bad were excluded from the analysis. Three-component traces in which only one scalar component passed the preliminary quality test were included in the data analysis, but only this 1C trace was analyzed. Yet, if a 3C trace contains two or three good components, it is possible to subsequently use the method of principal components (the polarization analysis). Principal components of such 3C traces are calculated for each of the wavelet-packet frequency bands (6).

For each αth wavelet-packet frequency band, the principal component is calculated in a moving time window of the radius $m_p T^{(\alpha)}_{\max}$, where m_p is a parameter of the algorithm and $T^{(\alpha)}_{\max}$ is the maximum period of the wavelet packet band (in units of the sampling interval; see the table). For each position of the moving time window, we calculated a sample estimate of the covariance matrix 2×2 or 3×3 in size (depending on how many scalar components passed the quality test), found the eigenvector corresponding to the maximum eigenvalue, and calculated the projection of the 2- or 3-D vector of seismic vibrations onto this eigenvector. The result of this procedure, the principal component of the 1C trace, is saved only for the central point of the moving time window. For the first window, adjacent to the beginning of the record, the principal component is saved for the time moments in the first half of the window (including the central point); for the last window,

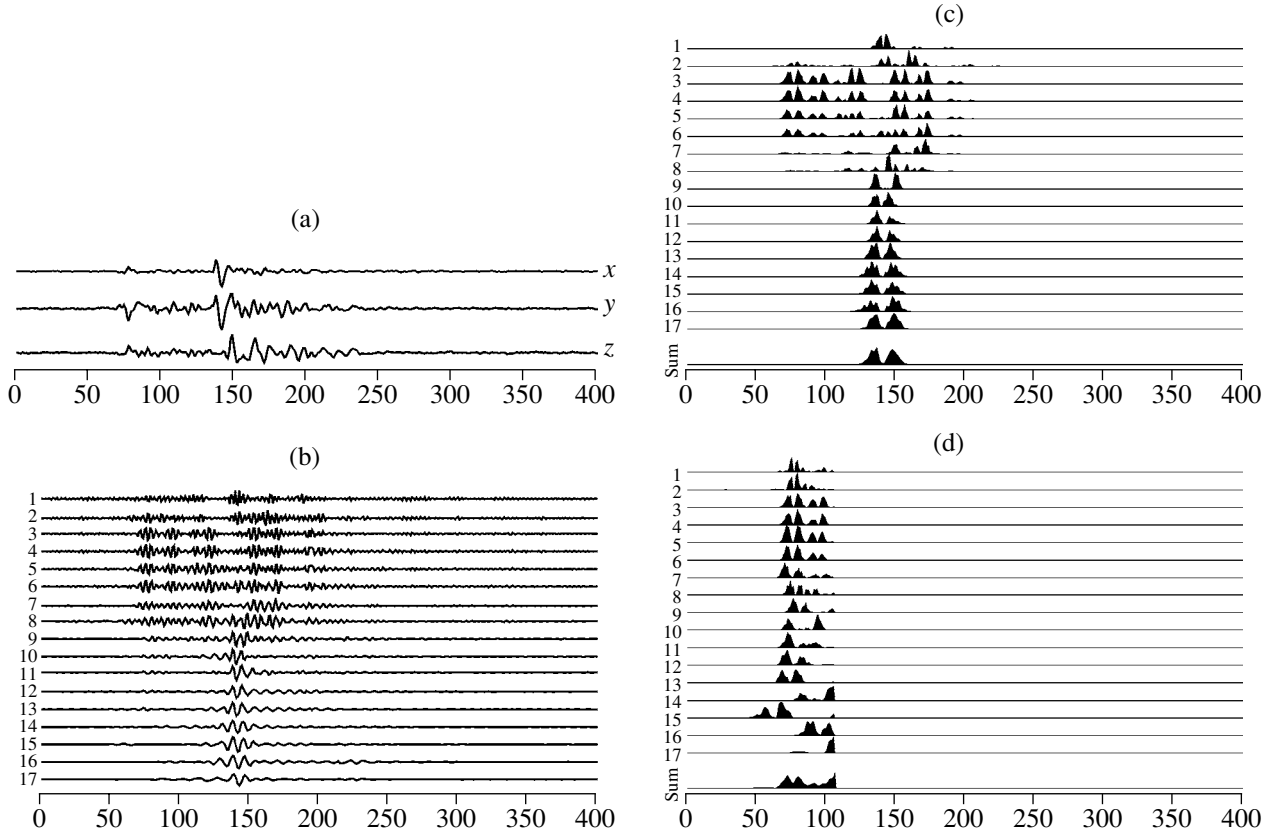

Fig. 4. (a) Good 3C trace no. 21. (b) Its principal components in 17 overlapping wavelet-packet frequency bands six octaves wide. (c) Behavior of nonstationarity measures in each frequency band; the lower plot (marked as "Sum") is the sum of the nonstationarity measures over all frequency bands and demonstrates the presence of arrival signals dominated by the *S* wave. (d) The same plot as in Fig. 4c but constructed for times that strictly precede *S* arrivals and are diminished by δt_S; the lower plot (marked as "Sum") is the sum of the nonstationarity measures over all frequency bands and is used for the detection of the *P* wave arrival.

adjacent to the end of the record, it is saved for the second half of the window. Figures 4a and 4b present the good 3C trace no. 21 and its principal components in all wavelet-packet frequency bands; Figs. 5a and 5b present similar plots for the partially good 3C trace no. 43.

5. Multilevel measures of nonstationarity for principal components. The measures of nonstationary behavior of a scalar trace introduced above by formulas (7) and (8) can be calculated in a similar way for scale-dependent principal components of each 3C trace. We denote these measures by $\mu_j^{(\alpha)}(\tau)$ and $\mu_j(\tau)$; the index k for distinguishing the *X, Y,* and *Z* components is omitted because it is unnecessary in this case. If a 3C trace has only one good 1C component, the measure used for this trace is calculated earlier by formulas (7) and (8). Figures 4c and 5c plot the dependences $\mu_j^{(\alpha)}(\tau)$ and $\mu_j(\tau)$.

6. Initial estimates of *S* wave arrival times. The method first determines *S* wave arrival times because they are, on average, more intense and are, therefore, easier to detect. Let j denote the number of a good or a partially good 3C trace; i.e., it is possible to analyze the statistic $\mu_j(\tau)$. Furthermore, let ξ be the center of the time window of radius equal to $M_b = 1.5T_{\max}^{(\alpha_{\max})}$ samples used for the analysis of variations in the statistic $\mu_j^{(\alpha)}(\tau)$. We emphasize that the formula for M_b contains the maximum period for the last, lowest frequency wavelet-packet band numbered $\alpha_{\max}$. Let $\bar{\mu}_j$ denote the average of $\mu_j(\tau)$ calculated over all τ values, and let $\nu_j(\xi)$ be the average of $\mu_j(\tau)$ calculated in a moving time window centered at the point ξ. The method for determining the initial estimates of *S* wave arrivals is based on the identification of time moments at which $\nu_j(\xi)$ exceeds the threshold $\rho\bar{\mu}_j$, which is equal to the product of the general average value of $\bar{\mu}_j$ and a coefficient ρ. The values of ρ range from 2 to 3 and are taken at a fairly small constant step. Note that, in some traces, *P* waves can have an energy comparable to or even

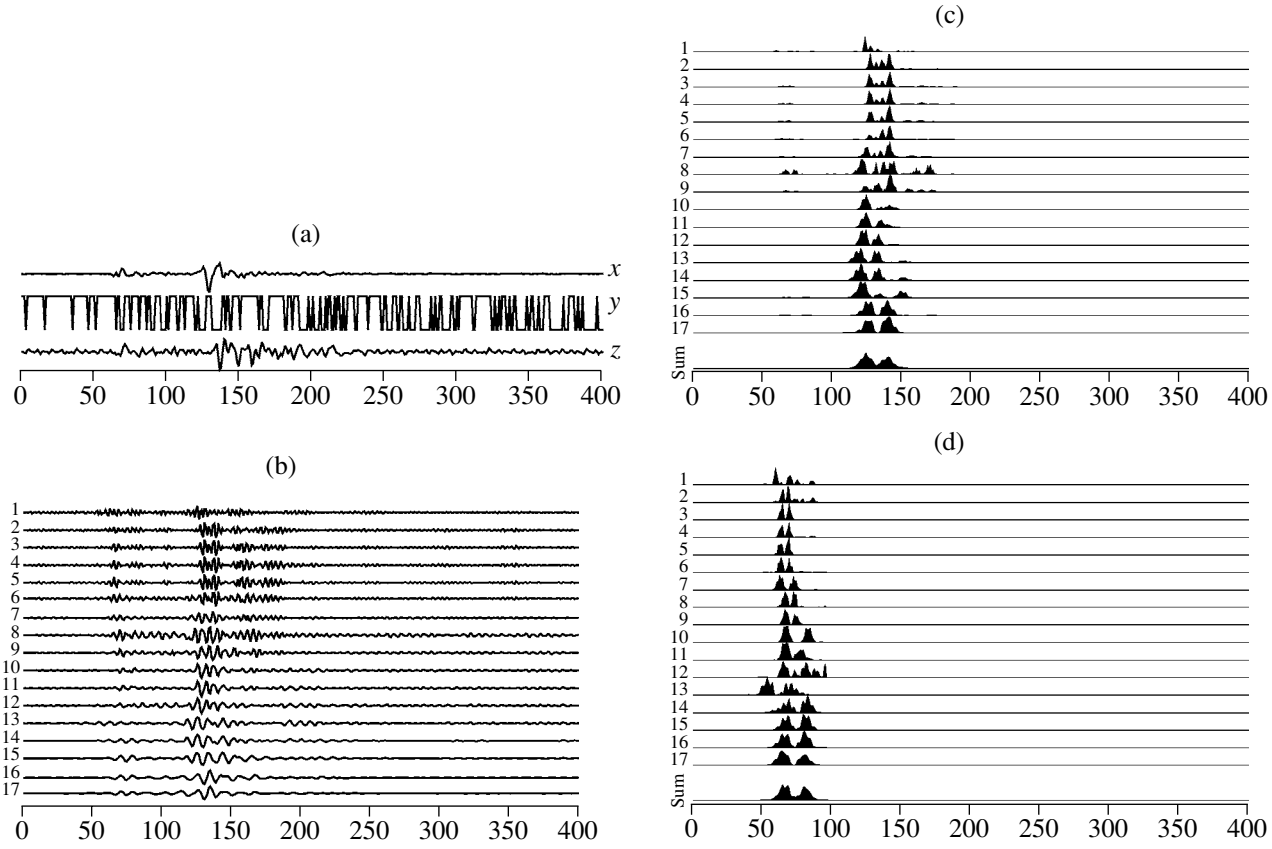

Fig. 5. (a) Partially good 3C trace no. 43. (b) Its principal components in 17 overlapping wavelet-packet frequency bands six octaves wide. (c) Behavior of nonstationarity measures in each frequency band; the lower plot (marked as "Sum") is the sum of the nonstationarity measures over all frequency bands and demonstrates the presence of arrival signals dominated by the *S* wave. (d) The same plot as in Fig. 5(c) but constructed for times that strictly precede the arrival of *S* waves and are diminished by δt_s; the lowermost plot (marked as "Sum") is the sum of nonstationarity measures over all frequency bands and is used for the detection of *P* wave arrival.

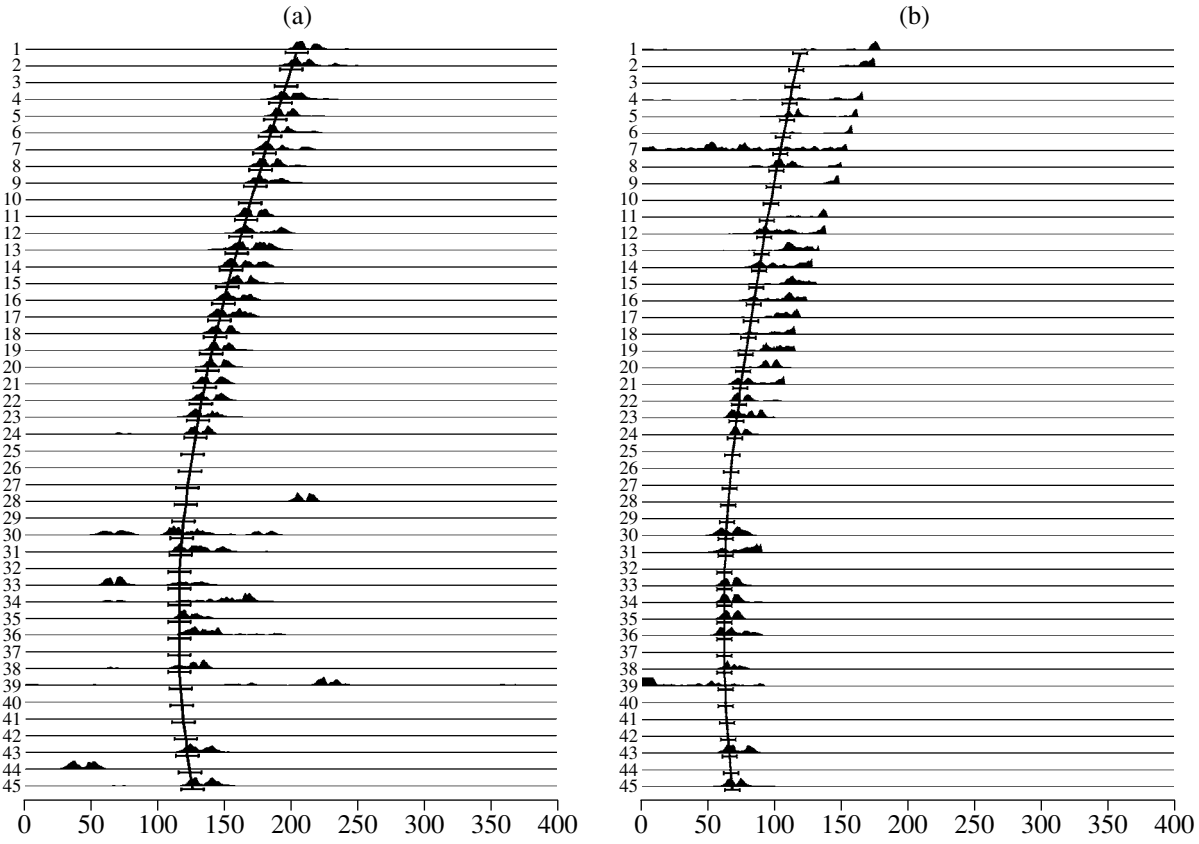

Fig. 6. Traveltime curves of (a) *S* and (b) *P* wave arrivals, with horizontal bars showing determination errors. Plot (a) shows the variations in the multilevel statistic for all traces that were not classified as "completely bad" at the first stage of automatic quality control; (b) the same measures of nonstationarity but constructed for times that strictly precede the arrival of *S* waves and are diminished by δt_s are shown for all traces that were not classified as "completely bad" at the second stage of quality control.

higher than that of *S* waves. To avoid misidentification of *P* wave arrivals as *S* wave arrivals in these cases, the analysis of peak values of the statistic $\mu_j(\tau)$ is applied *backward in time*, from the end of the record to its beginning. Thus, the time window moves from the end of the time interval to its beginning and the *first* position ξ_j^* of the window center ξ, such that $\nu_j(\xi) > \rho\bar{\mu}_j$, is sought for. The method then seeks the *first* time moment $\tau_j^* \in [\xi_j^* - M_b, \xi_j^*]$ of the first half of the moving window such that $\mu_j(\tau)$ exceeds 85% of the quantile of the distribution of $\mu_j(\tau)$ within the interval $t \in [\xi_j^* - M_b, \xi_j^* + M_b]$. We should emphasize that τ_j^* also depends on the coefficient ρ used to determine the threshold for moving averages of $\nu_j(\xi)$. Therefore, we write $\tau_j^* = \tau_j^*(\rho)$. The optimum value of the parameter ρ is found from the minimum variability condition for values of $\tau_j^*(\rho)$ between adjacent traces:

$$\sum_j \left|\tau_j^*(\rho) - \tau_{j-1}^*(\rho)\right| \longrightarrow \min_\rho, \quad \rho \in [2, 3]. \qquad (15)$$

The values of $\tau_j^*(\rho)$, where ρ is found by solving problem (15), are taken as the initial estimates of *S* wave arrival times along the *j*th traces.

7. Estimation of the *S* wave traveltime curve. The initial estimates of *S* wave arrival times are refined by an iterative self-organizing procedure for the adjustment of hyperbolic traveltime curves. A model hyperbolic traveltime curve is determined by the formula [Hatton et al., 1986]

$$T_j^* = \sqrt{T_0^2 + (s(j - j_0))^2}, \qquad (16)$$

where T_j^* is the model value of the arrival time, *j* is the number of the trace, and (T_0, s, j_0) are model parameters, with *s* being the wave slowness. The model parameters are found from the solution of the problem

$$\sum_j \left|(\tau_j^*)^2 - (T_j^*)^2\right| \longrightarrow \min_{T_0, s, j_0}. \qquad (17)$$

No correction is required for initial estimates of τ_j^* that lie within ±3 of the median distribution of the $|\tau_j^* - T_j^*|$ values in the neighborhood of the model traveltime

curve with the parameters determined from (17). However, values of τ_j^* lying outside this range are subjected to a correction procedure: they are replaced by the τ values that correspond to maximums of the statistic $\mu_j(\tau)$ for the arguments τ that lie within the above range. After this correction, the adjustment procedure (17) is repeated until it is no longer necessary to correct all values of τ_j^*. If the initial estimates of τ_j^* are more than ± 4 medians away from the model traveltime curve, these traces are classifies as bad and are excluded from the analysis; this is the second, final stage of the automatic quality control. The traces rejected at the second stage are marked in Fig. 1 by a double exclamation mark "!!."

If the traveltime curve with parameters adjusted by (17) has a minimum within the profile, i.e., $1 < j_0 < N_{\text{tr}}$, the neighborhood of the trace j_0 is unfavorable for applying the method of principal components because it contains strongly correlated noise from the near *P* wave arrival. In this situation, the use of variations in the measures $\mu_{j,k}(\tau)$ for individual scalar components can give a more accurate determination of the *S* arrival as compared with the use of the measure $\mu_j(\tau)$ for the principal component. Thus, for good or partially good 3C traces with the number j such that $|j - j_0| < 5$, the iterative method of correcting and adjusting the hyperbolic traveltime curve includes an analysis of peak values of the statistics $\mu_{j,k}(\tau)$ for the good scalar components k together with peak values of the statistics $\mu_j(\tau)$ for the principal component. In comparing these statistics, preference is given to the one for which the 85% quantile of variations in the measures realizes the minimum distance from the model traveltime curve after adjusting its parameters; it is precisely this value that is taken for correction (if it is necessary).

8. Initial estimates of *P* wave arrival times. *P* wave arrival times are sought after the determination of the *S* wave traveltime curve. The method is quite similar to the determination of the *S* wave traveltime curve, except that the initial estimates of *P* arrival times are sought from variations in the statistics $\mu_j(\tau)$ not for all values of τ but only for those that satisfy the inequality

$$\tau < t_s^{(j)} - 2T_{\max}^{(\alpha_{\max})} \equiv t_s^{(j)} - \delta t_s, \qquad (18)$$

where $t_s^{(j)}$ is the time of the *S* wave traveltime curve along the *j*th trace. Figures 4d and 5d plot the measures $\mu_j^{(\alpha)}(\tau)$ and $\mu_j(\tau)$ for the time moments $\tau \le t_s^{(j)} - \delta t_s$ used to determine the initial estimates of *P* arrival times. Note that the plots in Figs. 4d and 5d correspond to the same variations as in Figs. 4c and 5c, but they are not visible against the background of the much stronger variations associated with *S* arrivals. Only the construction of plots at the times $\tau \le t_s^{(j)} - \delta t_s$ made the preceding variation distinguishable.

9. Estimation of *P* wave traveltime curves. The *P* wave traveltime curve is determined by the same method of iterations with adjusting the model of the hyperbolic traveltime curve as that used for *S* waves, but the *P* wave slowness to be determined should not exceed the previously found *S* wave slowness divided by $\sqrt{2}$. Figure 6 shows plots of both traveltime curves along with their errors amounting to three-median deviations of the initial estimates from the final *S* and *P* traveltime curves.

To summarize, the full list of parameters of the method is as follows:

(1) p, the number of octaves in overlapping wavelet-packet frequency bands;

(2) $\alpha_{\max}$, the maximum number of wavelet packet bands;

(3) $\kappa_{\max}$, the threshold for the application of criterion (10) of automatic quality control;

(4) $\text{En}_{\max}$, the threshold for the application of entropy criterion (12);

(5) $\lambda_{\max}$, the threshold for the application of energy criterion (12); and

(6) m_p, the parameter defining the radius of the scale-dependent moving time window for the calculations of the principal components.

CONCLUSIONS

A method is developed and tested for the automatic identification of *P* and *S* wave arrival times in problems of passive seismic monitoring in borehole seismics with a low signal-to-noise ratio and numerous defective single-component traces. The method combines the ideas of wavelet-packet decomposition of seismic records and polarization analysis. The newly developed ideas of the automatic classification of defective traces and the accumulation of useful information by calculating the sum of variations in multilevel measures of nonstationarity can find use in monitoring problems of weak seismic events.

ACKNOWLEDGMENTS

This work was supported by the Schlumberger Cambridge Research Center. I am grateful to David Leslie for useful discussions and comments.

REFERENCES

1. C. K. Chui, *An Introduction to Wavelets* (Academic, San Diego, 1992; Mir, Moscow, 2001).
2. I. Daubeshies, *Ten Lectures on Wavelets* (SIAM, Philadelphia, 1992; NIts Reg. Khaotich. Dinamika, Izhevsk, 2001).
3. A. N. Gashin and A. F. Kushnir, "Traveling Anomalies of Regional Seismic Phases from Data of the Small-Aperture Alibek Array," in *Problems of Geodynamics and*

Seismology (Computational Seismology, issue 30) (Moscow, 1998), pp. 316–335 [in Russian].

4. L. Hatton, M. H. Worthington, and J. Makin, *Seismic Data Processing. Theory and Practice* (Blackwell, London, 1986; Mir, Moscow, 1989).
5. E. R. Kanasewish, *Time Series Analysis in Geophysics* (Univ. Alberta, 1981; Nedra, Moscow, 1985).
6. A. F. Kushnir and L. M. Khaikin, "Automated Data Processing for Seismic Monitoring with the Use of a Small-Aperture Array," in *Problems of Dynamics and Seismicity of the Earth (Computational Seismology, issue 31)* (Moscow, 2000), pp. 273–289 [in Russian].
7. A. A. Lyubushin, "Wavelet-Aggregated Signal and Synchronous Peaked Fluctuations in Problems of Geophysical Monitoring and Earthquake Prediction," Fiz. Zemli, No. 3, 20–30 (2000) [Izvestiya, Phys. Solid Earth **36**, 204–213 (2000)].
8. A. A. Lyubushin, "A Robust Wavelet-Aggregated Signal for Geophysical Monitoring Problems," Fiz. Zemli, No. 9, 37–48 (2002) [Izvestiya, Phys. Solid Earth **38**, 745–755 (2002)].
9. A. A. Lyubushin, Z. Kalab, and N. Chastova, "Application of Wavelet Anomaly to the Automatic Classification of Three-Component Seismic Records," Fiz. Zemli, No. 7, 50–56 (2004) [Izvestiya, Phys. Solid Earth **40**, 587–593 (2004)].
10. S. Mallat, *A Wavelet Tour of Signal Processing* (Academic, San Diego, 1998).
11. S. C. Maxwell, R. Bossu, R. P. Young, and J. Dangerfield, "Processing of Induced Microseismicity Recorded in the Ekofisk Reservoir," in *Annual Meeting Abstracts, Society of Exploration Geophysicists* (1998), pp. 904–907.
12. S. C. Maxwell, T. I. Urbancic, S. D. Falls, and R. Zinno, "Real-Time Microseismic Mapping of Hydraulic Fractures in Carthage, Texas," in *Expanded Abstracts. Society of Exploration Geophysicists. Session: RC2.9* (2000).
13. V. F. Pisarenko, A. F. Kushnir, and I. V. Savin, "Statistical Adaptive Algorithms for Estimation of Onset Moments of Seismic Phases," Phys. Earth Planet. Inter. **47**, 4–10 (1987).
14. W. H. Press, B. P. Flannery, S. A. Teukolsky, and W. T. Vettering, *Numerical Recipes*, 2nd ed. (Cambridge Univ. Press, Cambridge, 1996), Chap. 13.
15. *Seismic Signal Analysis and Discrimination. Methods in Geochemistry and Geophysics*, Ed. by C. H. Chen (Elsevier, Amsterdam, 1982; Mir, Moscow, 1986).
16. R. J. Zinno, J. Gibson, R. N. Walker, Jr., and R. J. Withers, "Overview: Cotton Valley Hydraulic Fracture Imaging Project," in *Annual Meeting Abstracts. Society of Exploration Geophysicists* (1998), pp. 926–929.